J. Fluid Mech. (2012), *vol.* 708, *pp.* 377–396.
doi:10.1017/jfm.2012.315

Models for inviscid wakes past a normal plate

A. Elcrat[1] **and L. Zannetti**[2]†

[1] Wichita State University 1845 N. Fairmount, Wichita, KS 67260-0033, USA

[2] DIMEAS, Politecnico di Torino, Corso Duca degli Abruzzi 24, 10129 Torino, Italy

(Received 26 April 2012; revised 26 April 2012; accepted 19 June 2012;
first published online 14 August 2012)

Closed and open hollow wakes are considered as analytic models for the two-dimensional inviscid steady flow past a plate normal to the stream. It is shown that only open configurations which satisfy the Kutta condition exist. The main argument is based on considering a plate located on the edge of a step with varying height. It is shown that solutions for open wakes exist for backward-, null and forward-facing steps, while closed wakes only exist for backward-facing steps. The occurrence of secondary separation has been modelled by adding a hollow region attached to the downstream corner. Peculiar accuracy issues of the problem are pointed out which may explain other contradictory results from the literature. It is shown how the Kirchhoff wake is a limiting solution for certain values of the governing parameters.

Key words: separated flows, vortex dynamics, wakes

1. Introduction

Inviscid steady solutions for the flow past bluff bodies are relevant to wake control and to the asymptotic theory of separated flows in the limit of the Reynolds number going to infinity. It is often assumed that steady flows with recirculation regions with closed streamlines are useful in stabilizing unstable steady flows at high Reynolds numbers (see Protas 2008). The general discussion can be illuminated by consideration of a particular geometry where specialized methods can be applied. This work aims to do this for the intriguing and controversial features of two-dimensional inviscid models of the wake past a flat plate normal to the flow. This simple geometry is the one which was used in the first wake model using free streamlines, on which the magnitude of the velocity is constant, Kirchhoff (1869) (and for instance, Lamb 1932).

The inviscid flow model is characterized by flow constrained to separate from the sharp edges of the plate (Kutta condition) and by an arbitrary distribution of vorticity inside the wake. In general, the wake can have a finite area with closed streamlines, as in the Batchelor (1956*b*) wake model, or can extend to infinity, as in the Kirchhoff wake model. A rich discussion and bibliography on this argument is offered, for instance, by Chernyshenko (1998) and Sychev *et al.* (1998).

The inviscid two-dimensional steady flow is governed by the quasi-linear Poisson equation $\nabla^2\psi = -\omega(\psi)$, where ψ is the stream function and ω the vorticity. Different models are characterized by different choices of the function $\omega(\psi)$; by assuming the wake formed by vortex patches bounded by vortex sheets, it becomes

$$\omega = -\sum_j \omega_j H(\psi - \alpha_j) + \sum_k \beta_k \delta(\psi - \gamma_k) \tag{1.1}$$

† Email address for correspondence: luca.zannetti@polito.it

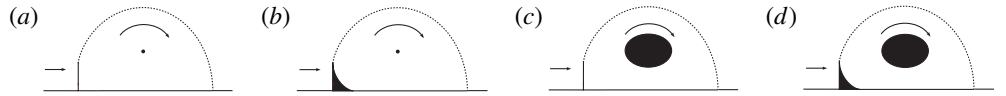

FIGURE 1. Closed hollow wake models.

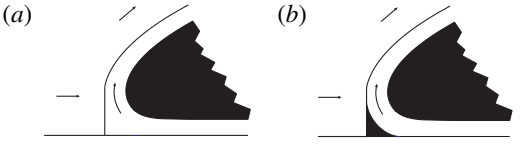

FIGURE 2. Open hollow wake models.

where H and δ denote the Heaviside and Dirac functions, respectively, α_j and γ_k are the values of the stream function at the patch boundaries and on the vortex sheets, ω_j is the vortex patch vorticity and β_k the jump of the Bernoulli constant across the vortex sheets. Batchelor (1956*a*) showed that the steady inviscid limit of a region with closed streamlines, for the Reynolds number $Re \to \infty$, is a vortex patch bounded by a vortex sheet, which belongs to this general wake model.

'Hollow wake' models are adopted here; they are based on assuming $\omega_j = 0$. As a consequence the vorticity is concentrated on vortex sheets which bound irrotational regions. For $\psi = \text{const.}$ on the wake boundary, irrotationality implies, by the maximum principle for the Laplace equation, $\psi = \text{const.}$ inside the wake, which thus is 'hollow', that is, formed by fluid at rest . The point vortex model is included in this scenario, it corresponds to letting $|\gamma_k| \to \infty$. Sychev *et al.* (1998) considered this model as a generalization of the Batchelor model and attributed it to Lavrentiev (1962).

This model has the merit that it allows a fully, or almost fully, analytic study which avoids most of the uncertainties of other approaches. Examples of studies based on this model have been recently offered by Crowdy & Green (2011), Telib & Zannetti (2011) and Llewellyn Smith & Crowdy (2012).

We explore two classes of wake models: one pertinent to finite-area wakes with closed streamlines and the other one pertinent to open wakes which extend, *a la* Kirchhoff, to infinity. Figures 1 and 2 summarize the patterns considered for the two classes. They are schematic. Indeed, the main result of this work is that the fulfillment of the Kutta condition makes the patterns of figure 1, pertinent to closed wakes, unlikely to exist.

Figure 1(*a*) is pertinent to the point vortex model; in figure 1(*b*) a hollow region is added in the corner to model the effect of a secondary separation, in figures 1(*c*) and 1(*d*) the point vortex is desingularized into a hollow region. Figures 2(*a*) and 2(*b*) show the considered open wakes models, without and with a secondary separation, respectively.

The non-existence of inviscid closed wakes for a normal flat plate has been recently discussed in the literature. Since the non-existence of a solution in which the wake vorticity is concentrated on a point vortex is known (Smith & Clark 1975), continuation arguments, as those by Gallizio *et al.* (2010), imply that finite-area desingularized solutions do not exist either. This result is controversial. In fact, there are several examples in the literature which contradict it. For instance, Turfus (1993) studied the problem, equivalent to the present one, of a normal plate in a channel

and found a solution with a finite-area vortex patch. Gallizio (2004) considered the same problem and arrived at the opposite result. Alimov & Mazo (2002) considered the same flow in an unbounded domain and found a solution which satisfies the Kutta condition, but they stated difficulties in accurately enforcing the Kutta condition. Lin & Landweber (1977) computed a finite-area hollow wake according to the model of figure 1(*c*), but their result has been refuted by Telib & Zannetti (2011).

We here present further arguments in favour of the non-existence thesis, and we show how the counterexamples in the literature could be affected by inaccuracy inherent to peculiar aspects of the problem.

For two-dimensional potential flows, the inverse problem of determining the shape of streamlines along which the velocity distribution is prescribed can in general be solved by the hodograph-plane method.

The method consists of determining the function $z(\lambda)$ which maps a suitably chosen canonical domain of the parameter λ-plane onto the flow domain of the physical z-plane. Briefly, it is based on exploiting the chain rule $\mathrm{D}\{w(z(\lambda))\} = w'(z)z'(\lambda)$, rearranged as

$$\frac{\mathrm{d}z}{\mathrm{d}\lambda} = \frac{\mathrm{d}w/\mathrm{d}\lambda}{\mathrm{d}w/\mathrm{d}z}, \tag{1.2}$$

where $z = x + \mathrm{i}\,y$ is the complex coordinate of the physical z-plane, w is the complex potential and λ is the complex coordinate of the parameter plane. Let $\tau = \mathrm{d}w/\mathrm{d}z$ be the complex coordinate of the hodograph $\mathrm{d}w/\mathrm{d}z$-plane, then the shape of the flow field boundary on the τ-plane, that is, the velocity distribution along the boundary, is provided by the formulation of the inverse problem. The solution is obtained by conformally mapping the domain of the τ-plane onto a canonical domain of the parameter λ-plane. Once the complex velocity $\mathrm{d}w/\mathrm{d}z$ is expressed as a function of λ, the right-hand side of (1.2) is a known function of λ and the mapping function $z(\lambda)$ can be obtained by integration.

It should be remarked here that this process depends on the velocities on the boundary tracing out relatively simple curves in the τ-plane. If the geometry is polygonal then the boundary in the τ-plane consists of straight lines and circular arcs corresponding to the free streamlines, but even then the situation can be complicated. For fairly simple objects the domain in the τ-plane may be a Riemann surface, as in Elcrat (1982).

The canonical domain of the λ-plane can be arbitrarily chosen. For a simply connected flow domain, typical choices are half-planes, disks and rectangles. They lead to equivalent solutions by the Riemann mapping theorem. A large number of examples and variations on the method can be found in the literature; Gurevich (1965), for instance, is a rich source on this matter.

2. A point vortex behind a step

We begin with an example which can be solved directly analytically. This will serve to set notation and give the context for our main work. The physical configuration is given in figure 3.

We have a vertical flat plate *BC* with a backward-facing step *BD* in a uniform flow from left to right. There is a point vortex at *V* and we enforce a Kutta condition at the top of the plate at *C*. The streamline emanating from *C* reattaches to the horizontal behind the step at *F*. In a careful formulation of this problem we find things that might

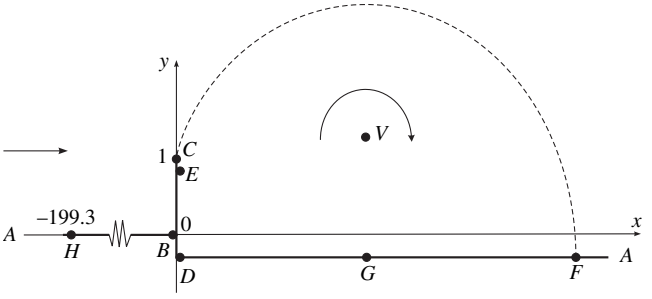

FIGURE 3. Physical plane for a point vortex.

not have been anticipated. On the streamline AB there is a maximum speed, larger than the speed at infinity (A), normalized to be $q_A = 1$, which is taken on at the point H. In the recirculation region $CFGDC$ there is necessarily a maximum speed at a point G between F and D, but there is also a maximum speed larger than the separation speed at C located at a point E on DC. The existence of these points E, G and H will play an essential role in our subsequent discussion. The above picture holds whether or not the vortex is in equilibrium. We will vary the location of the coordinates of V in order to achieve equilibrium. Figure 3 is an actual flow configuration, not a schematic.

If we map the flow domain onto the upper half of the λ-plane, the Schwarz–Christoffel formula with $\lambda = -1, 0, a, \infty$ corresponding to B, C, D, A respectively yields

$$\frac{\mathrm{d}z}{\mathrm{d}\lambda} = b\frac{\lambda}{\sqrt{(\lambda+1)(\lambda-a)}} \tag{2.1}$$

and, by integration,

$$z = b\left[\sqrt{(\lambda+1)(\lambda-a)} + \frac{a-1}{2}\log(1-a+2\lambda+2\sqrt{(\lambda+1)(\lambda-a)}) + c\right], \tag{2.2}$$

where c, b, a are defined by $z_B = 0$, $|z_C - z_B| = 1$ and by the free selection of step height BD.

The complex potential w can be defined in the λ-plane as the combination of a uniform flow, a point vortex plus its mirror image. By assuming as reference velocity the flow velocity at infinity, it is

$$w = b\,\lambda + \frac{\gamma}{2\pi\mathrm{i}}\log\left(\frac{\lambda-\lambda_v}{\lambda-\overline{\lambda}_v}\right), \tag{2.3}$$

where $\lambda_v = \xi_v + \mathrm{i}\eta_v$ is the vortex location and γ is the vortex circulation. The complex velocity on the λ-plane is thus

$$\frac{\mathrm{d}w}{\mathrm{d}\lambda} = b + \frac{\gamma}{2\pi\mathrm{i}}\left(\frac{1}{\lambda-\lambda_v} - \frac{1}{\lambda-\overline{\lambda}_v}\right). \tag{2.4}$$

The Kutta condition $(\mathrm{d}w/\mathrm{d}\lambda)_0 = 0$ yields

$$\gamma = -b\,\pi\,\frac{\xi_v^2+\eta_v^2}{\eta_v}. \tag{2.5}$$

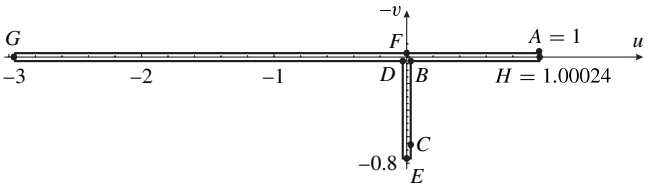

FIGURE 4. Hodograph for the point vortex.

According to the Routh (1881) rule (see also Clements 1973), the vortex velocity

$$\dot{\bar{z}}_v = \lim_{z\to z_v}\left(\frac{\mathrm{d}w}{\mathrm{d}z} - \frac{\gamma}{2\pi\mathrm{i}}\frac{1}{z-z_v}\right) \tag{2.6}$$

can be expressed as

$$\dot{\bar{z}}_v = \left(\bar{\lambda}'_v - \frac{\gamma}{4\pi\mathrm{i}}\frac{\mathrm{d}}{\mathrm{d}\lambda_v}\log\frac{\mathrm{d}z_v}{\mathrm{d}\lambda_v}\right)\frac{\mathrm{d}\lambda_v}{\mathrm{d}z_v}, \tag{2.7}$$

with

$$\bar{\lambda}'_v = \lim_{\lambda\to\lambda_v}\left(\frac{\mathrm{d}w}{\mathrm{d}\lambda} - \frac{\gamma}{2\pi\mathrm{i}}\frac{1}{\lambda-\lambda_v}\right) = b - \frac{\gamma}{2\pi\mathrm{i}(\lambda_v - \bar{\lambda}_v)}. \tag{2.8}$$

The equation which expresses the equilibrium of a vortex which satisfies the Kutta condition is thus

$$\bar{\lambda}'_v - \frac{\gamma}{4\pi\mathrm{i}}\frac{\mathrm{d}}{\mathrm{d}\lambda_v}\log\frac{\mathrm{d}z_v}{\mathrm{d}\lambda_v} = 0, \tag{2.9}$$

with $\bar{\lambda}'_v$ and γ given by the above equations.

The step in the above can in principle be any positive number (recall BC is normalized to be 1). We may also consider a zero step and a forward-facing step in which CD is smaller than BC. Following the same approach as in Zannetti (2006), we have plotted the zero-level curves for the real and imaginary parts of the function in (2.9) in various cases. For the backward-facing step these curves cross at a unique point, but, as BD is made smaller, determination of the crossing point becomes delicate. When the step is zero the two curves are parallel. When the step transitions to forward facing the curves diverge. Hence, there is no equilibrium position for a point vortex behind a forward-facing step as well as for the previously known case of a zero step.

We can get insight into the dependence on parameters by observing the values of the velocities at equilibrium q_E, q_G and q_H. In particular, the value of q_H is significant. Consider the hodograph or complex velocity plane for these flows shown in figure 4. In this figure the hodograph domain is the exterior of the T-shaped curve, and we see that the velocity at H is $q_H = 1.00024$, barely above the free-stream velocity $q_A = 1$. Further, the location of H in the z-plane is very far upstream as shown in figure 3 ($z_H = -199.3$). We see that q_H depends sensitively on the step length; the value $q_H = 1.00024$ considered here is relevant to the step $BD = 0.3$.

It is possible to give an analysis of these 'steps with point vortex' flows in channels. (The Kutta condition is imposed, but equilibrium is left aside.) With reference to the physical and hodograph planes shown in figure 5, when the step is zero ($d = d'$) the asymptotic upstream and downstream velocities are $q_A = q_{A'} = 1$. As the top wall

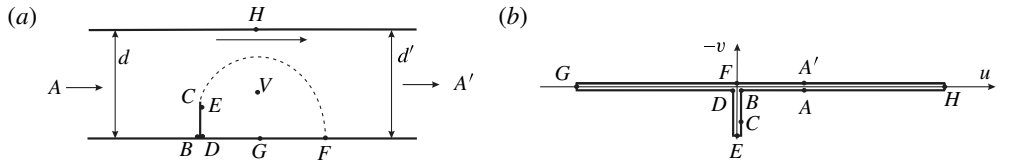

FIGURE 5. (*a*) Physical and (*b*) hodograph planes for a point vortex in a channel (equilibrium not imposed).

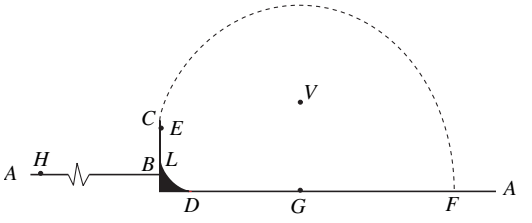

FIGURE 6. Flow past a point vortex and corner vortex.

recedes to infinity, we find that the geometry implies that the limiting value of q_H must be $q_H = q_A = q_{A'} = 1$.

3. Hollow corner vortices and desingularization of point vortices by hollow vortices

3.1. *Point vortices with hollow corner vortices*

We proceed now to investigate the configuration shown in figure 1(*b*). Our intent is to investigate how the results of a point vortex behind a step change when a 'hollow' vortex, i.e. a zero flow region, is added to simulate secondary separation on the corner at the plate base *D*. This is inspired by Turfus & Castro (2000), who considered secondary separation in their inviscid model for the flow past a cascade of plates.

We begin with a hollow corner added at the corner as shown in figure 6. The problem is normalized by taking the plate length *CB* and the velocity at infinity q_A as reference values. As before there is a point vortex at *V* and the Kutta condition is imposed at *C*, but now the streamline coming back from *G* detaches before the corner at *D* and reattaches on the plate at *L*. Bernoulli's equation implies that the speed *q* is constant on this 'free streamline' *DL*. This problem cannot be solved directly, but we will give a solution using the classical hodograph method. We assume a plausible geometry for the hodograph and find the physical domain as an inverse problem in which parameters are adjusted. The hodograph here is the exterior domain in the τ-plane depicted in figure 7. An essential role is played by the velocity maxima that we found for a point vortex which we now assume for the corner flow. We may think of q, q_E, q_G and q_H as free parameters. We approximate the circular arc *LD* by a polygon with $N = 40$ vertices, and use a variant of the Schwarz–Christoffel transformation to map the exterior domain into the unit disk of the λ-plane. The

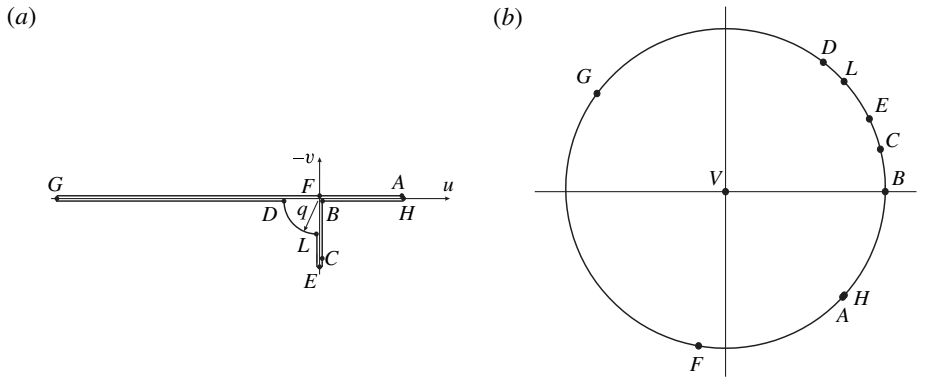

FIGURE 7. (*a*) Hodograph for the flow past a point vortex and corner vortex. (*b*) λ-plane.

mapping is thus

$$\tau = A + C\int^{\lambda} \nu^{-2} \prod_k \left(1 - \frac{\nu}{\lambda_k}\right)^{1-\alpha_k} \mathrm{d}\nu, \tag{3.1}$$

where λ_k are the locations of the 'prevertices' and $\pi\alpha_k$ are the polygon angles. This transformation has been computed using SCTOOLBOX (Driscoll 1996).

The mapping is such that $\tau = \infty$, that is, the point vortex, is mapped onto the centre $\lambda_v = 0$ of the unit disk and the stagnation point $\tau_B = 0$ is mapped onto $\lambda_B = 1$. This allows the values of the constants A and C and of the prevertices λ_k to be determined.

The complex velocity $\mathrm{d}w/\mathrm{d}\lambda$ is given by the combination of a doublet at $\lambda = \lambda_A$, representative of the asymptotic uniform flow in the physical plane, and by a vortex located at $\lambda = \lambda_v = 0$. By adjusting the doublet orientation to make the unit circle a streamline, we have

$$\frac{\mathrm{d}w}{\mathrm{d}\lambda} = Q\left[\frac{\mathrm{i}\,\lambda_A}{(\lambda - \lambda_A)^2} + \frac{\gamma/Q}{2\pi\mathrm{i}\,\lambda}\right], \tag{3.2}$$

where Q is the momentum of the doublet and γ is the circulation of the vortex. In (1.2), Q plays the role of a scale factor and its value can be adjusted *a posteriori* to set the unit length of the plate. At $\lambda = \lambda_F$, $\tau_F = 0$, since for the physical wall to be regular at F, $(\mathrm{d}z/\mathrm{d}\lambda)_F$ must be finite, and, hence $(\mathrm{d}w/\mathrm{d}\lambda)_F = 0$. This defines the circulation $\gamma/Q = -\pi/\sin^2[(\varphi_F - \varphi_A)/2]$, with $\varphi_F = \arg(\lambda_F)$ and $\varphi_A = \arg(\lambda_A)$. The complex velocity $\mathrm{d}w/\mathrm{d}\lambda$ has a second zero in $\lambda_C = \exp[\mathrm{i}\,(2\,\varphi_A - \varphi_F)]$; this defines the λ image of the edge C of the plate and the velocity $\tau_C = \tau(\lambda_C)$.

As derived in the Appendix, (2.9), which expresses the equilibrium of the vortex, assumes the form

$$\frac{A}{C} + \frac{2\pi}{\gamma/Q\,\lambda_A} = 0. \tag{3.3}$$

This is a complex equation and its satisfaction reduces to two the degrees of freedom of the problem. Accordingly, we organize the computations as follows: the two degrees of freedom are represented by the free choice of the velocity q_H and of the velocity ratio q/q_E, then q and q_G are determined so that the vortex is in equilibrium. We have computed solutions for a range of values of q_H and q/q_E. Note that $0 \leqslant q/q_E \leqslant 1$,

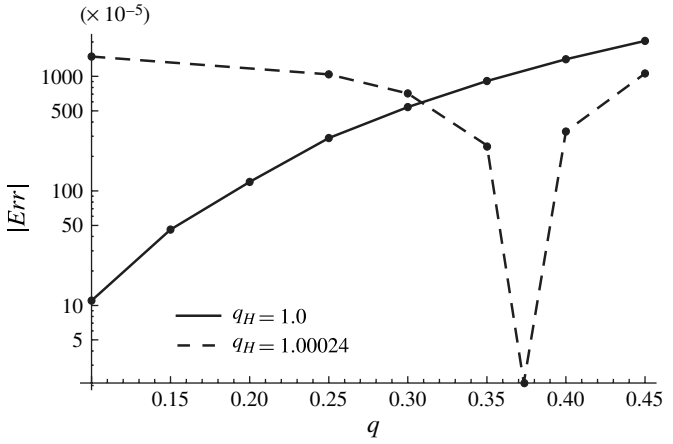

FIGURE 8. Error versus q for $q/q_E = 0.5$ and $q_H = 1$ and $q_H = 1.00024$.

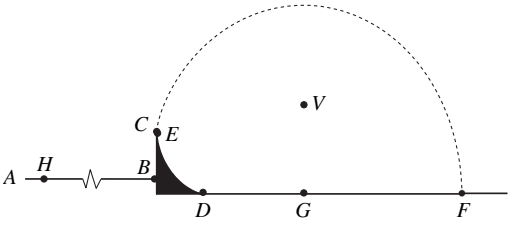

FIGURE 9. A corner vortex with $q/q_E = 1$ ($q = 0.5597$, $q_G = 2.9483$, $q_C = 0.5363$).

the limiting cases being no corner vortex and maximum possible speed on the corner vortex boundary.

This combination was arrived at after much trial and error, and we have formulated a check on the correctness of our solution based on these experiments. In figure 8 we have plotted the magnitude of the minimum error for values of q_G with q fixed. For $q_H > 1$ the geometry results in a positive step and there is a clear indication of a minimum which is consistent with the error passing through zero. For $q_H = 1$ the geometry corresponds to a zero step. Here the magnitude of the error becomes fairly small but does not have a minimum. Moreover, as the error decreases, the vortex moves towards downstream infinity. We take this as an indication that a solution for equilibrium does not exist. Our first computations converged for such cases if the accuracy requested was modest, say 10^{-3}, but we were not able to get smaller errors. We believe that results such as those in figure 8 explain this.

In conclusion, the answer to the question of whether including the corner vortex makes a zero step possible is no. The argument follows the same line as for a point vortex without a corner vortex. By considering related flows in channels we can deduce that q_H must be 1 when the step is 0, and for $q_H = 1$ the above analysis shows that there is no solution.

We have found a direct relation between q/q_E and the size of the corner vortex. This is illustrated in figures 9 and 10.

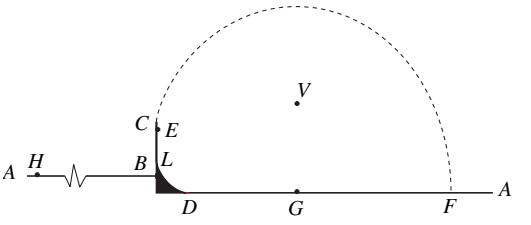

FIGURE 10. A corner vortex with $q/q_E = 0.5$ ($q = 0.3733$, $q_G = 2.9517$, $q_C = 0.6491$).

3.2. *Desingularization of point vortices by hollow vortices.*

We consider now the flow pattern shown in figure 1(*c*), where the point vortex is desingularized in a finite-area hollow. The resulting wake model coincides with the Lavrentiev (1962) model; it consists of a layer of potential flow which surrounds a body of fluid at rest. If the Kutta condition is satisfied, there is a single infinity of solutions which depends on the free choice of the constant velocity q_h along the hollow boundary.

This flow has been studied by Lin & Landweber (1977), who used a hodograph-plane method and found solutions for the zero-step case. Recently, Telib & Zannetti (2011) have proposed a different method and have cast doubts on the existence of those solutions. Further arguments are presented here.

Lin & Landweber (1977) used a hodograph method in which the *BD* step height is part of the solution. According to an iterative method, they used the zero-step constraint to tune the parameters on which the solution depends. We show here how this constraint is delicate and a very small violation may induce a false solution. Moreover, in their hodograph method the Kutta condition is implicitly satisfied and solutions which violate it cannot be explored.

The method by Telib & Zannetti (2011) is a direct rather than an inverse formulation. In that method the shape of the solid wall is fixed and is not part of the solution; this means that the step height *BD* is set *a priori* and is not the result of a trial and error process. Moreover, the Kutta condition can be explicitly enforced and can be violated as well. In Telib & Zannetti (2011) a zero step was assumed, and it was shown that solutions with wakes with the lengths given by Lin & Landweber (1977) violated the Kutta condition.

To provide further arguments, we here adopt that same method for non-zero-step configurations by using the mapping (2.2). We show that the behaviour of the solutions for decreasing step heights suggests that zero-step solutions are unlikely to exist.

An example of a solution for a non-zero step is shown in figure 11. In the same figure the point vortex solution is also represented. The hollow wake separatrix is represented by a solid line and the point vortex separatrix by a dotted line. For the plate length *CB* taken as reference length, the solutions pertinent to three different steps ($BD = 0.51,\ 0.16,\ 0.06$) are compared in figure 12. As the step height is decreased, the wake lengths increase and the hollow vortices move downstream with strongly nonlinear behaviour. It can be deduced that, as for the point vortex solution, the hollow location and the wake length tend to infinity as *BD* goes to zero. In a numerical approach, solutions with quite small values of *BD* could be mistaken as an indication of existence of a solution for $BD = 0$.

Moreover, if, instead of the plate length *BC*, we assume as reference length the wake length, we can also deduce that the zero-step ($BD = 0$) solution is pertinent to a

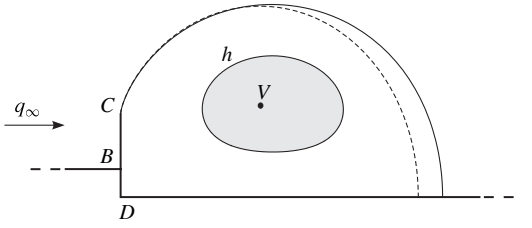

FIGURE 11. Hollow wake ($q_h = 3$) past a normal plate with a positive step ($BD = 0.51$).

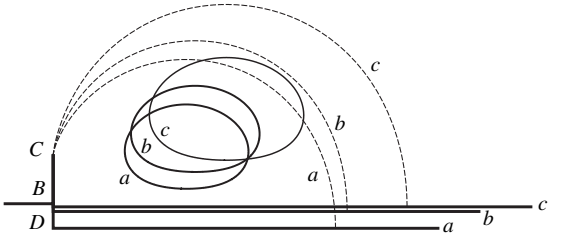

FIGURE 12. Hollow wakes for $q_h = 3$ and $BD = 0.51,\ 0.16,\ 0.06$ (a,b,c).

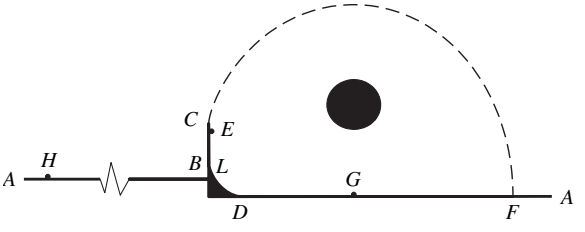

FIGURE 13. Closed hollow wake with hollow corner separation ($q_H = 1.00024,\ q/q_E = 0.5,\ q_h = 7$).

plate with vanishing length ($BC = 0$) and it coincides with the finite-area hollow vortex above an infinite flat wall found by Pocklington (1895).

For given BD, the solutions depend on the free choice of $q_h > 1$. As for the other wall geometries considered by Telib & Zannetti (2011), the method fails to converge for small values of q_h. We have not been able to detect if there is a limit value different from $q_h = 1$, which pertains to the Kirchhoff wake.

3.3. *Closed hollow wake with secondary corner separation*

We consider now the flow of figure 13, which shows a solution pertinent to the pattern shown in figure 1(d), where the point vortex of § 3.1 is desingularized by a hollow vortex. The hodograph is as depicted in figure 14. A magnification of the details in (a) are shown in b). It consists of a doubly connected domain where the inner boundary has the same T-shape as for the above point vortex case (figure 7) and the outer boundary is a circle whose radius q_h is the velocity along the hollow vortex standing in the wake core.

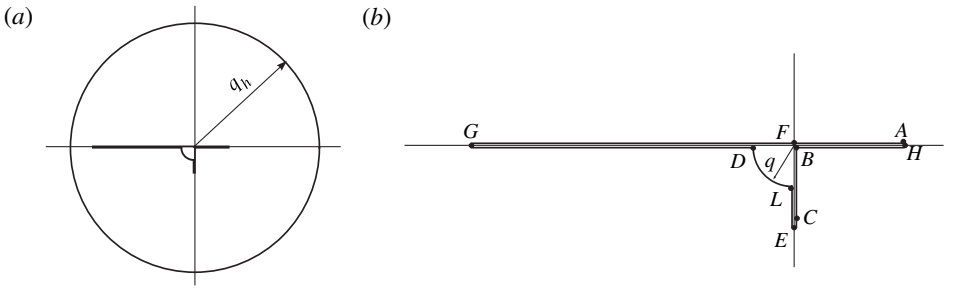

FIGURE 14. Hodograph for the closed vortex: (*a*) doubly connected domain, (*b*) inner profile.

As above, the inner profile is defined by the maxima of the wall velocity (q_H, q_E, q_G) and by the q velocity along the corner hollow separation. In addition to q, q_H, q_E, q_G, the problem now depends also on the q_h value of the flow velocity at the hollow vortex boundary. We follow the same hodograph method as in § 3.1, with the variation that the doubly connected domain of the hodograph-plane domain is mapped conformally onto an annulus of the λ-plane. With this mapping function in hand, an inverse problem can be formulated for the determination of the flow domain in the physical plane. A system of two equations for closure of the hollow vortex can be given which replaces the system for equilibrium of the point vortex. For given values of q_H, q_h and q/q_E, the independent variables are again q and q_G, and the same equation solving routine is used.

The mapping onto the annulus is done in two steps. First, the Schwarz–Christoffel mapping (3.1) is used to define the function $\tau(\lambda_1)$ which maps the domain external to the profile of figure 14(*b*) into the interior of the unit disk of the intermediate λ_1-plane. The doubly connected hodograph is thus mapped onto a doubly connected region of the λ_1-plane, bounded by the unit circle and by the quasi-circular image of the q_h circle. The Garrick (1936) mapping, as formulated by Ives (1976)

$$\lambda_1 = \lambda \exp\left\{ \mathrm{i}\, b_0 + \sum_{n=1}^{N-1} [(-a_n + \mathrm{i}\, b_n)\,(R\lambda)^n + (a_n + \mathrm{i}\, b_n)\,(R/\lambda)^n] \right\}, \tag{3.4}$$

is then used to map this region into an annulus of the λ-plane bounded by the unit circle and by an inner circle with radius R. The a_n, b_n coefficients and radius R are computed by the iterative process suggested by Ives (1976).

In order to define the complex velocity $\mathrm{d}w/\mathrm{d}\lambda$, it is convenient to consider the further mapping $\chi = \log \lambda$. On the χ-plane the hodograph domain is mapped onto the rectangular region bounded by thick lines in figure 15. According to the geometrical periodicity of the horizontal sides and to the infinite reflections needed to make the vertical side streamlines, the function $\mathrm{d}w/\mathrm{d}\chi$ has to be a doubly periodic elliptic function with a second-order pole at χ_A to represent the uniform flow at infinity. The periodic domain is shown in figure 15; its half-periods are $\omega = -\log R$ and $\omega' = \mathrm{i}\,\pi$. From $\lambda(\mathrm{d}w/\mathrm{d}\lambda) = \mathrm{d}w/\mathrm{d}\chi$, the complex velocity on the λ-plane is thus

$$\frac{\mathrm{d}w}{\mathrm{d}\lambda} = \frac{\mathrm{i}\,Q}{\lambda}[\wp(\log\lambda - \chi_A; \omega, \omega') + \kappa)], \tag{3.5}$$

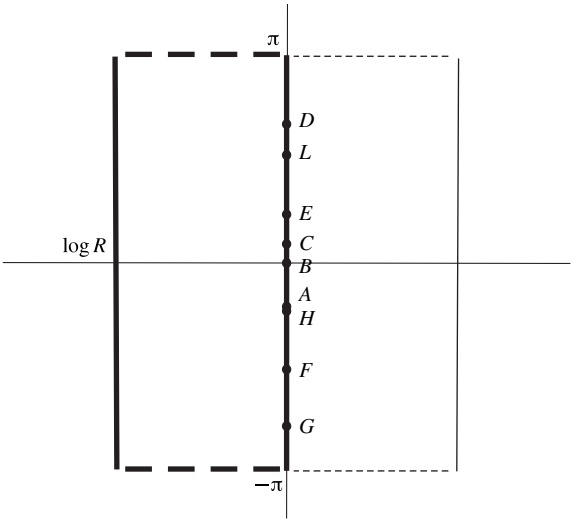

FIGURE 15. χ-plane.

where $\wp$ is the Weierstrass $\wp$ function. The value of κ is determined by the location of the stagnation point χ_F, that is, $\kappa = -\wp(\chi_F - \chi_A)$. As a consequence of the properties of the zeros of the elliptic functions, $\mathrm{d}w/\mathrm{d}\chi = 0$ also at $\chi_C = 2\,\chi_A - \chi_F$, which defines the $\lambda_C = \exp\chi_C$ location of the λ-image of the plate edge C. According to (1.2), Q plays the role of a scale factor and its value is determined *a posteriori* to enforce the plate length $CB = 1$.

According to (1.2), the function $\mathrm{d}z/\mathrm{d}\lambda$ can now be determined. The condition that the hollow vortex has to be closed is expressed by the complex equation

$$\oint_{|\lambda|=R} \frac{\mathrm{d}z}{\mathrm{d}\lambda}\,\mathrm{d}\lambda = 0, \tag{3.6}$$

which allows the unknown values of q and q_G to be computed.

The same arguments as used above for channel flow can be used to show that the zero step corresponds to $q_H = 1$. We have performed the same numerical check as in § 3.1 and obtained a confirmation of that result. In figure 16, as in figure 8, we have plotted the magnitude of the minimum error $|Err|$ for values of q_G with q fixed. For $q_H > 1$ the geometry results in a positive step and there is a clear indication of a minimum which is consistent with the error passing through zero. For $q_H = 1$ the geometry corresponds to a zero step. Here the magnitude of the error becomes fairly small but does not have a minimum. The figure is relevant to $q/q_E = 1$ and $q_h = 7$. The same behaviour was seen for other values of the parameters that we have explored.

Figure 17 presents two examples of solutions with the same $q_H = 1.00024$ value and with different values of $0 \leqslant q/q_E \leqslant 1$ and $q_h > 1$. It shows how the hollow corner region, the hollow wake core and the wake length depend on these parameters. The general indication is that wake length increases as q_h decreases, and one would expect that for $q_h \to 1$ the wake approaches the Kirchhoff wake, but, as in § 3.2, the failure of the method for small values of q_h did not allow this outcome to be verified.

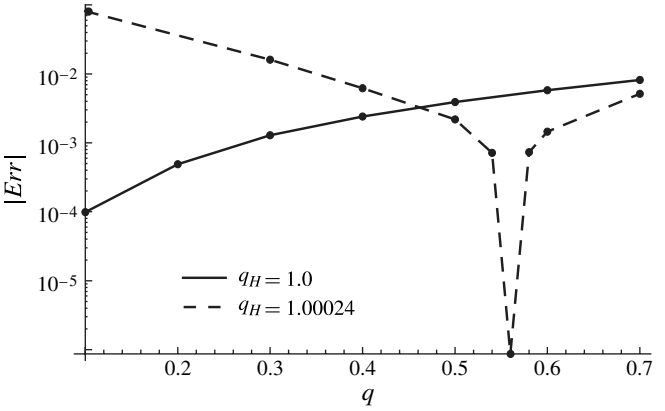

FIGURE 16. Error versus q for $q/q_E = 1$ and for $q_H = 1$ and $q_H = 1.00024$.

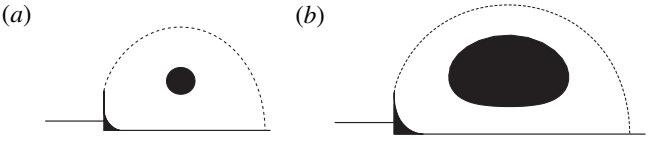

FIGURE 17. Examples of closed wakes: (*a*) $q_H = 1.00024$, $q/q_E = 0.5$, $q_h = 7$; (*b*) $q_H = 1.00024$, $q/q_E = 1$, $q_h = 2.7$.

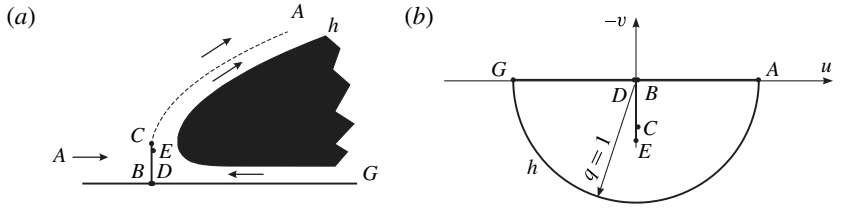

FIGURE 18. Open hollow wake without corner separation: (*a*) physical plane; (*b*) hodograph plane.

4. Normal plate and infinite hollow wakes

We consider now two models for infinite open wakes past a normal plate. First we will consider the case without secondary separation, and then we will include, as above, a hollow region on the downstream corner to model a secondary separation. The solution is obtained by means of the hodograph method. As shown below, these models are capable of describing wakes for negative, null or positive steps.

4.1. *Open wakes without secondary corner separation*

The flow in the physical plane is shown in figure 18(*a*). The wake consists of an infinite hollow region bounded by a layer of potential flow. The relevant hodograph on the τ-plane is shown in 18(*b*). It consists of a half unit circle with a cut extending from the origin B to the maximum velocity q_E attained along the plate. As above, this maximum velocity in general does not coincide with the velocity q_C at the plate

edge C. The problem is normalized by assuming as reference velocity the velocity q_A at infinity and the length CB of the plate. By assuming uniform pressure at infinity, the hollow pressure has to be equal to the pressure at infinity and, as a consequence, the constant velocity q on its boundary has to be equal to the velocity at infinity, that is $q = q_A = 1$. Note that the hodograph geometry depends on the single parameter $0 \leqslant q_E \leqslant 1$.

The hodograph can be mapped onto a rectangle by the Jacobi sine-amplitude function. Therefore it is convenient to adopt this rectangle, traced by thick lines in figure 19, as the canonical domain in the transformed λ-plane. The mapping is

$$\tau = -\mathrm{i}\, q_E \,\mathrm{sn}(\lambda, m), \tag{4.1}$$

where the parameter m is found by solving the implicit equation

$$\mathrm{sn}\left[\frac{\mathrm{i}}{2}K(1-m), m\right] = \frac{\mathrm{i}}{q_E}, \tag{4.2}$$

and K is the complete elliptic integral of the first kind.

The complex velocity $\mathrm{d}w/\mathrm{d}\lambda$ has to be such that the sides of the rectangle result as streamlines. As a consequence, it is a doubly periodic function whose periodic domain is shown in the figure by dotted lines. To represent the uniform flow at infinity, a quadrupole has to be located in λ_A; the flow in the potential layer from G to A has to be represented by a source in λ_G and a sink in λ_A. By enforcing periodicity, the complex velocity is thus the elliptic function

$$\frac{\mathrm{d}w}{\mathrm{d}\lambda} = M\{\wp'(\lambda - \lambda_A; \omega, \omega') + Q[\zeta(\lambda - \lambda_G; \omega, \omega') - \zeta(\lambda - \lambda_A; \omega, \omega') + \kappa]\}, \tag{4.3}$$

where the Weierstrass functions $\wp'$ and ζ have been introduced, and the half-periods are $\omega = 2\lambda_E$ and $\omega' = \lambda_A$. From (1.2), M plays the role of a scale factor and it can be set *a posteriori* to enforce the plate length $CB = 1$. Since $\wp'(-\lambda_A) = 0$, the condition that B is a stagnation point yields $\kappa = \zeta(\lambda_G) - \zeta(\lambda_A)$. The constant Q represents a further degree of freedom of the problem, its value defines the location of the λ_C image of the plate edge C. By enforcing the Kutta condition $(\mathrm{d}w/\mathrm{d}\lambda)_C = 0$, the relationship between Q and λ_C is

$$Q = -\frac{\wp'(\lambda_C - \lambda_A)}{\zeta(\lambda_C - \lambda_G) - \zeta(\lambda_C - \lambda_A) + \kappa}. \tag{4.4}$$

From the physical point of view, the quantity $\dot{m} = (\pi/2)\, M\, Q$ is the mass flow in the wake potential layer. Geometrically, by using (1.2), for a given q_E, Q defines the step height BD, which can be positive (backward-facing step), null (flat plane) or negative (forward-facing step). In the examples shown here, it has been adjusted to attain a null step $BD = 0$.

By integrating $\mathrm{d}w/\mathrm{d}\lambda$, the complex potential

$$w = M\left\{\wp(\lambda - \lambda_A; \omega, \omega') + Q\left[\log\frac{\sigma(\lambda - \lambda_G; \omega, \omega')}{\sigma(\lambda - \lambda_A; \omega, \omega')} + \kappa\lambda\right]\right\}, \tag{4.5}$$

results, where the $\wp$ and σ Weierstrass functions have been introduced. Figure 19 shows the streamline pattern on the λ-plane for the zero-step case displayed in figure 18(*a*), relevant to $q_E = 0.5$.

In conclusion, the open wake past a normal plate orthogonal to a zero-step plane has one degree of freedom represented by the free choice of $0 \leqslant q_E \leqslant 1$. As shown

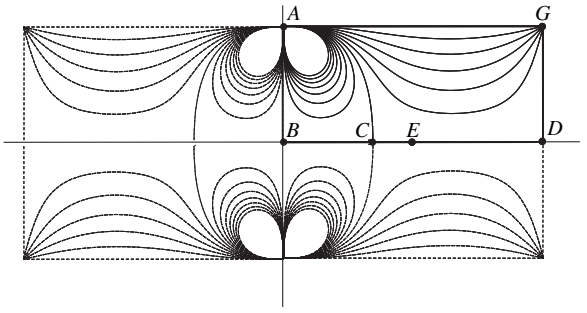

FIGURE 19. Transformed λ-plane for an infinite hollow wake without corner separation.

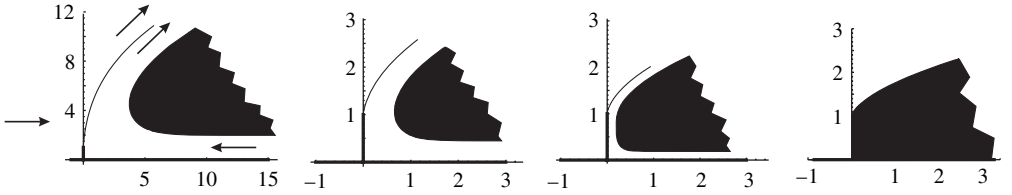

FIGURE 20. Infinite hollow vortices and their limiting case, $q_E = 0.1, 0.5, 0.95, 1$.

in figure 20, pertinent to $q_E = 0.1, 0.5, 0.95, 1$, the distance of the hollow from the plate is a monotonic decreasing function of q_E. For $q_E = 1$, the above hodograph degenerates onto a quarter-circle, and the solution is the Kirchhoff wake. The other limit is $q_E = 0$, for which the cut BE on the hodograph half-circle disappears and the distance of the hollow from the plate goes to infinity. By assuming as reference length the distance of the hollow from the plate, we see that $q_E = 0$ corresponds to a plate with a vanishing length, that is, the resulting flow is the flow which separates from a point C of a flat plane and generates an infinite recirculating region with a hollow core. As for the Kirchhoff wake, this flow has been known for a long time; for instance, it was considered by Michell (1890) and Pocklington (1895).

While, according to the d'Alembert's paradox, inviscid closed wakes have zero drag, open wakes can experience non-null drag. In figure 21 the drag coefficient C_D, pertinent to the present model, is plotted versus the parameter q_E. It is an increasing function of q_E which goes from $C_D = 0$ for $q_E = 0$ to $C_D = 0.88$ for the limiting Kirchhoff wake ($q_E = 1$).

4.2. *Open wakes with secondary corner separation*

We consider now the flow represented in figure 22, in which a hollow corner region has been added to model a secondary separation at the corner. This flow model presents a further degree of freedom represented by the value q of the velocity on the boundary of the corner hollow vortex. The pertinent hodograph τ-plane is shown in figure 23(a); by taking $\log \tau$, the hodograph is mapped onto the polygon shown in figure 23(b), with the vertex B located at infinity. The Schwarz–Christoffel mapping is then used to map the interior of the polygon onto the upper half-λ-plane, as shown in

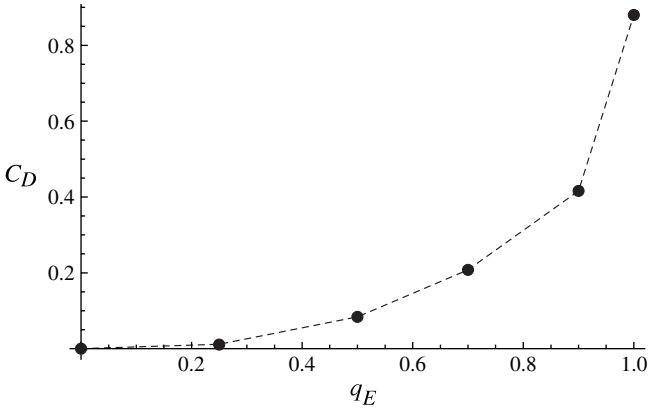

FIGURE 21. C_D versus q_E for open hollow wakes.

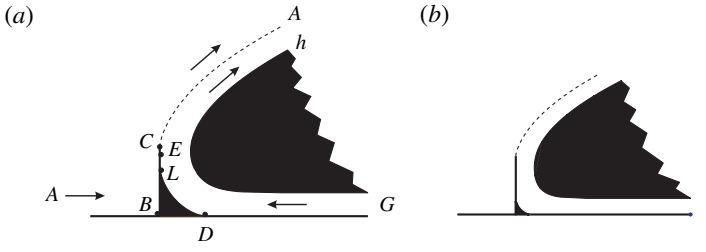

FIGURE 22. Open hollow wakes with secondary corner separation: (*a*) $q_E = 0.62$, $q = 0.496$; (*b*) $q_E = 0.8$, $q = 0.240$.

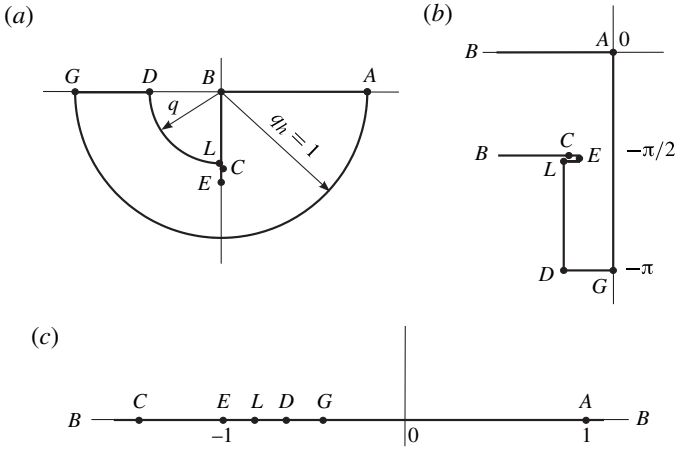

FIGURE 23. Open hollow wake with secondary corner separation: (*a*) hodograph τ-plane; (*b*) log τ-plane; (*c*) λ-plane.

figure 23(*c*). The $\lambda \to \tau$ mapping is thus

$$\tau = \exp\left[A + C\int^{\lambda} \prod_k (\nu - \lambda_k)^{\alpha_k - 1}\, \mathrm{d}\nu\right], \tag{4.6}$$

where λ_k are the polygon λ-prevertices and $\pi\alpha_k$ the angles. By assuming $\lambda_B = \infty$, $\lambda_E = -1$ and $\lambda_A = 1$, the values of the other prevertices and of the constants A and C are uniquely determined. The computation has been carried out by means of the Driscoll (1996) SCTOOLBOX.

The complex velocity $\mathrm{d}w/\mathrm{d}\lambda$, is the velocity induced by a doublet located in λ_A, representing the asymptotic uniform flow, and by a source in λ_G and a sink in λ_A, representing the flow in the wake potential layer, that is

$$\frac{\mathrm{d}w}{\mathrm{d}\lambda} = M\left[\frac{1}{(\lambda - \lambda_A)^2} + Q\left(\frac{1}{\lambda - \lambda_G} - \frac{1}{\lambda - \lambda_A}\right)\right]. \tag{4.7}$$

As in § 4.1, M is a scale factor which can be set *a posteriori* to enforce the unit length of the plate, and Q is a parameter whose value defines the location of the separation point, that is, of the image λ_C of the plate edge. From $(\mathrm{d}w/\mathrm{d}\lambda)_C = 0$, we get

$$Q = -\frac{1}{(\lambda_C - \lambda_A)^2[1/(\lambda_C - \lambda_G) - 1/(\lambda_C - \lambda_A)]}. \tag{4.8}$$

Physically, $\dot{m} = \pi M Q$ is the mass flow in the wake potential layer. For given values of the free parameters $0 < q_E < 1$ and $0 < q \leqslant q_E$, the value of Q defines the step height BD, which can be positive, null or negative. In our computations, we adjusted it in order to attain a null step.

Figure 22 shows two cases with different values of q_E and q. In case (*a*), the mass flow in the potential layer is $\dot{m} = 0.336$ and in case (*b*) it is $\dot{m} = 0.276$. As for the $q = 0$ case of § 4.1, the limit for $q_E \to 1$ appears to be the Kirchhoff wake, with $\dot{m} = 0$.

5. Conclusions

We have considered inviscid hollow wake models for the flow past a normal plate, with and without secondary corner separation. The closed wake models summarized in figure 1 have been shown not to exist. The main argument is based on considering the plate located on the edge of a step with varying height. It has been shown that closed wakes only exist for positive, backward-facing steps.

The limiting flow configuration for a vanishing step is the Pocklington (1895) hollow vortex standing above a flat plane.

Other results from the literature, which contradict the present ones, can be explained by the peculiar accuracy aspects of the problem, which are related to the fulfillment of the Kutta condition and of the zero-step requirement.

This outcome gives support to the thesis, based on continuation arguments as in Gallizio *et al.* (2010), that the non-existence of a wake modelled by a point vortex implies the non-existence of desingularized solutions.

It has been shown that, according to the patterns of figure 2, solutions exist for open wakes modelled by infinite hollow regions, with and without a secondary corner separation. By varying the free parameters $0 < q_E < 1$ and $0 \leqslant q \leqslant q_E$, which represent the maximum velocity attained on the plate and the velocity on boundary of the

hollow corner vortex, respectively, different solutions exist with different non-null values of the drag coefficient. The limiting cases are the Pocklington (1895) infinite hollow ($q_E = 0$) and the Kirchoff wake ($q_E = 1$).

In general, the Kirchhoff wake does not depend on the shape of the body downstream of the separation point. According to the present study, the Kirchhoff wake is relevant to given downstream geometries, so it is not an isolated solution, but it is the limiting case of a continuum of solutions.

Appendix. Computational procedures

In our exposition we have written little about the methods that we have used in computing our solutions in order not to distract attention from our main points. We will give more information here.

All of our work was done on our personal computers using the software packages Mathematica (2008) and MATLAB (2010). In §§ 2 and 4.1, the complete solutions were obtained analytically using Mathematica.

The $|Err|$ plots of figures 8 and 16 have been computed by means of the MATLAB (2010) routine fminbnd.m. For given q, it provides the value q_G which minimizes $|Err|$.

The hollow vortices depend on a conformal map of the hodograph domain onto either the interior of the unit disk when there is a point vortex or the interior of an annulus when there is a hollow vortex. For the former we use the exterior map option in the Matlab Toolbox SCTOOLBOX (Driscoll 1996). Using extermap.m, ∞ is mapped to the origin in the unit disk. The circular arc in the hodograph is approximated by a polygonal line with 40 segments.

Equation (3.3) follows from (2.9) with $\lambda_v' = \mathrm{i}\,Q/\lambda_A$ and

$$\begin{aligned}\frac{\mathrm{d}}{\mathrm{d}\lambda_v}\log\frac{\mathrm{d}z}{\mathrm{d}\lambda_v} &= \lim_{\lambda\to 0}\left(\frac{\mathrm{d}}{\mathrm{d}\lambda}\log\frac{\mathrm{d}w}{\mathrm{d}\lambda} - \frac{\mathrm{d}}{\mathrm{d}\lambda}\log\tau\right)\\ &= \lim_{\lambda\to 0}\left\{\left[-\frac{1}{\lambda} - \frac{2\pi}{\gamma/Q}\frac{\lambda_A}{(\lambda-\lambda_A)^2} + O(\lambda)\right] - \left[-\frac{1}{\lambda} - \frac{A}{C} + O(\lambda)\right]\right\}\\ &= \frac{A}{C} - \frac{2\pi}{\gamma/Q}\frac{1}{\lambda_A}\end{aligned} \tag{A 1}$$

where the expansion of the mapping (3.1)

$$\tau(\lambda) = A - \frac{C}{\lambda} + O(\lambda) \tag{A 2}$$

has been used. The value of the constant A is part of the Driscoll (1996) SCTOOLBOX output, while the value of the constant C has been evaluated from

$$C = -\frac{1}{2\pi\mathrm{i}}\oint \tau(\lambda)\,\mathrm{d}\lambda \tag{A 3}$$

by approximating the contour integral on $|\lambda| = 0.9$ using 300 G quadrature points. The accuracy of the prevertices obtained from SCTOOLBOX are of order 10^{-8} and we need only the prevertices of q_A and q_F to evaluate the objective function for determining equilibrium. Our tests indicate that we have sufficient accuracy in these parts to be confident of 6 places of accuracy in the objective function. We have used the Matlab routine fsolve.m to find the values of q/q_E and q_G at which equilibrium is achieved. The output indicates at least 6 decimal places of accuracy in the solution.

When the point vortex is desingularized to a hollow vortex we have found the hodograph, shown in figure 14, by mapping a circle around the origin in the point vortex hodograph to a quasi-circle inside the unit disk, and then performing Garrick (1936) iterations to map this quasi-annulus onto an annulus.

The computation has been done using MATLAB (2010). The Garrick (1936) mapping has been computed according to the Ives (1976) formulation. Let $\lambda_1 = r\exp(\mathrm{i}\,\vartheta)$ and $\lambda = \rho\exp(\mathrm{i}\,\varphi)$. Let $r = r_h(\vartheta)$ be the quasi-circular image of the hollow vortex on the λ_1 plane, then (3.4) yields

$$\log r_h = \log R + \sum_{n=1}^{N-1}(1-R^{2n})\,a_n\cos(n\varphi) + (1-R^{2n})\,b_n\sin(n\varphi), \tag{A 4}$$

$$\vartheta = \varphi + b_0 + \sum_{n=1}^{N-1}(1+R^{2n})\,b_n\cos(n\varphi) - (1+R^{2n})\,a_n\sin(n\varphi). \tag{A 5}$$

A distribution of $2N$ equispaced points have been taken on the unit circle of the λ-plane, with $N = 50$, and the values of (R, a_n, b_n) have been computed by fixed-point iteration: from (A 5), the inverse FFT provides $\vartheta_k = \vartheta(\varphi_k)$ $(k = 0, \ldots, 2N-1)$; from (A 4), the FFT on $\log(r_k) = \log[r_h(\vartheta_k)]$ provides new values for (R, a_n, b_n). The value of b_0 is free; it defines a solid rotation. We selected $b_0 = -\sum_{n=1}^{N-1}(1+R^{2n})\,b_n$ so that $\vartheta = 0$ corresponds to $\varphi = 0$.

The function $r = r_h(\vartheta)$ has been obtained by means of a cubic spline. The accuracy on the solution (Fourier coefficients) has been set to 10^{-9}.

MATLAB (2010) routines have been written to evaluate the Weierstrass elliptic functions. As in Tricomi (1951), they have been expressed by means of their relationships with the Jacobi ϑ_j functions, which have been coded according to their rapidly converging power series.

REFERENCES

ALIMOV, M. M. & MAZO, A. B. 2002 On the M. A. Lavrentyev model for stationary vortex zones. *Fluid Dyn.* **5**, 705–712.

BATCHELOR, G. K. 1956*a* On steady laminar flows with closed streamlines at large Reynolds number. *J. Fluid Mech.* **1**, 177–190.

BATCHELOR, G. K. 1956*b* A proposal concerning laminar wakes behind bluff bodies at large Reynolds number. *J. Fluid Mech.* **1**, 388–398.

CHERNYSHENKO, S. I. 1998 Asymptotic theory of global separation. *Appl. Mech. Rev.* **51**, 523–536.

CLEMENTS, R. R. 1973 An inviscid model of two-dimensional vortex shedding. *J. Fluid Mech.* **57**, 321–336.

CROWDY, D. G. & GREEN, C. C. 2011 Analytical solution for von Kármán streets of hollow vortices. *Phys. Fluids* **23**, 126602.

DRISCOLL, T. 1996 A MATLAB toolbox for Schwarz–Christoffel mapping. *ACM Trans. Math. Softw.* **22**, 168–186.

ELCRAT, A. 1982 Separated flow past a plate with spoiler. *SIAM J. Math. Anal.* **13**, 632–639.

GALLIZIO, F. 2004 Modello di Prandtl–Batchelor per il flusso normale ad una placca piana posta all'interno di un canale: studio numerico dell'esistenza e unicità della soluzione. Dissert. Tesi Laurea Ing. Aerosp. aa 2003/2004, Politecnico di Torino, Turin, Italy.

GALLIZIO, F., IOLLO, A., PROTAS, B. & ZANNETTI, L. 2010 On continuation of inviscid vortex patches. *Physica* D **239**, 190–201.

GARRICK, I. E. 1936 Potential flow about arbitrary biplane wing sections. *NACA Rep.* 542.

GUREVICH, M. I. 1965 *Theory of Jets in Ideal Fluids*. Academic.

IVES, D. C. 1976 A modern look at conformal mapping, including multiply connected regions. *AIAA J.* **14**, 1006–1011.

KIRCHHOFF, G. 1869 Zur theorie freier flussigkeitsstrahlen. *J. Reine Angew. Math.* **70**, 289–298.

LAMB, H. 1932 *Hydrodynamics*. Cambridge University Press.

LAVRENTIEV, M. A. 1962 *Variational Methods for Boundary Value Problems for Systems of Elliptic Functions*. Noordhoff.

LIN, A. & LANDWEBER, L. 1977 On a solution of the Lavrentiev wake model and its cascade. *J. Fluid Mech.* **79**, 801–823.

LLEWELLYN SMITH, S. G. & CROWDY, D. G. 2012 Structure and stability of hollow vortex equilibria. *J. Fluid Mech.* **691**, 170–200.

MATHEMATICA, 2008 *Mathematica, version 8.0*. Wolfram Research, Inc.

MATLAB, 2010 *version 7.10.0 (R2010a)*. The MathWorks Inc.

MICHELL, J. H. 1890 On the theory of free stream lines. *Phil. Trans. R. Soc. Lond.* A **182**, 394–431.

POCKLINGTON, H. C. 1895 The configuration of a pair of equal and opposite hollow straight vortices, of finite cross-section, moving steadily through fluid. *Proc. Camb. Phil. Soc.* **8**, 178–187.

PROTAS, B. 2008 Vortex dynamics models in flow control problems. *Nonlinearity* **21**, 203–250.

ROUTH, E. J. 1881 Some application of conjugate functions. *Proc. Lond. Math. Soc.* **12**, 73–89.

SMITH, J. H. B. & CLARK, R. W. 1975 Nonexistence of stationary vortices behind a two-dimensional normal plate. *AIAA J.* **13** (8), 1114–1115.

SYCHEV, V. V., RUBAN, A. I., SYCHEV, V. V. & KOROLEV, G. L. 1998 *Asymptotic Theory of Separated Flows*. Cambridge University Press.

TELIB, H. & ZANNETTI, L. 2011 Hollow wakes past arbitrarily shaped obstacles. *J. Fluid Mech.* **669**, 214–224.

TRICOMI, F. 1951 *Funzioni Ellittiche*. Zanichelli.

TURFUS, C. 1993 Prandtl–Batchelor flow past a flat plate at normal incidence in a channel – inviscid analysis. *J. Fluid Mech.* **249**, 59–72.

TURFUS, C. & CASTRO, I. E. 2000 Prandtl–Batchelor model of flow in the wake of a cascade of normal plates. *Fluid Dyn. Res.* **26**, 181–202.

ZANNETTI, L. 2006 Vortex equilibrium in the flow past bluff bodies. *J. Fluid Mech.* **562**, 151–171.